



Highly selective oxidation of glycerol over Bi/Bi_{3.64}Mo_{0.36}O_{6.55} heterostructure: Dual reaction pathways induced by photogenerated ¹O₂ and holes



Shuai Zhao^a, Zan Dai^a, Wenjin Guo^a, Fengxi Chen^a, Yunling Liu^b, Rong Chen^{a,*}

^a School of Chemistry and Environmental Engineering, Wuhan Institute of Technology, Wuhan 430073, PR China

^b State Key Laboratory of Inorganic Synthesis and Preparative Chemistry, College of Chemistry, Jilin University, Changchun 130012, PR China

ARTICLE INFO

Keywords:
 Bi/Bi_{3.64}Mo_{0.36}O_{6.55}
 Glycerol
 Selective oxidation
¹O₂
 Photogenerated hole

ABSTRACT

Selective oxidation of glycerol to produce aimed high-value added products is of great importance in chemical industry. Photocatalytic oxidation provides a promising and green strategy for selective glycerol oxidation. In this work, we develop a Bi/Bi_{3.64}Mo_{0.36}O_{6.55} heterostructure *via* a facile solvothermal method for the selective oxidation glycerol to 1, 3-dihydroxyacetone (DHA) in water under visible light irradiation. The excellent performance in activity and selectivity of Bi/Bi_{3.64}Mo_{0.36}O_{6.55} heterostructure for DHA production is attributed to a dual-pathway photocatalytic reaction process. The mass production ¹O₂ ascribed to the reduced energy gap (ΔE_{ST}), the enhanced spin-orbit coupling (SOC) and the presence of oxygen vacancy is beneficial for the selective oxidation of glycerol to DHA. Simultaneously, the metallic bismuth in the heterostructure promotes the separation of photogenerated holes with efficient redox potential and facilitates the binding bismuth with ortho-hydroxyl in glycerol, thus enhancing the yield and selectivity of DHA production. This work provides a novel strategy and thorough understanding of the development of highly efficient bismuth-based photocatalyst for selective oxidation in organic reactions.

1. Introduction

As a primary by-product from the production of biodiesel, the surplus glycerol has brought about a series of problems [1,2]. Therefore, the economics and sustainable development of biodiesel production requires the integrated utilization of glycerol [3–5]. Generally, the selective oxidation of glycerol could generate numerous industrially high-value added products such as 1, 3-dihydroxyacetone (DHA), glyceraldehyde (GAD), glyceric acid (GCA), lactic acid (LA), glycollic acid (GCOA), and formic acid (FA) [6–11] etc. (Scheme S1, Supporting Information). Among them, DHA is one of most important products due to its potential use in fine chemical industry, particularly in pharmaceutical and cosmetics [12,13]. However, due to the presence of three reactive hydroxyl groups, the highly selective oxidation of glycerol to DHA still remains a big challenge [14,15]. Besides microbial oxidation *via* fermentation process [16,17], the selective oxidation of glycerol *via* heterogeneous catalyst (*i.e.* Pd, Pt, Au based bi-metallic catalysts) [18–20] and homogenous catalyst (*i.e.* C₂₇H₃₁F₃IrN₃O₃S, C₂₁H₂₀F₃IrN₃O₅S, [Cp*Ir(IME)₂Cl]BF₄) [21,22] have been reported. Electrochemical approach has also realized the glycerol being

converted to DHA by using modified electrode [23,24]. Nevertheless, different obstacles such as long operation time, low selectivity and metal loss in the process are presented in their further applications. Currently, photocatalytic oxidation provides an appealing strategy for selective oxidation of alcohol and polyol [25]. For examples, selective glycerol oxidation to DHA was realized over flower-like Bi₂WO₆ under visible light irradiation [26]. Selective oxidation of alcohol using Bi₂MoO₆ as a photocatalyst also has been reported [27,28]. However, the unsatisfied photocatalytic performance of photocatalyst in selective glycerol oxidation still hinder the practical applications [29,30].

To overcome the obstacles of low photocatalytic efficiency and selectivity, the discovery or design of highly effective visible-light-driven photocatalysts for selective glycerol oxidation to DHA is particularly of great interest and importance. Recently, bismuth-based oxysalt has emerged as promising candidate owing to its unique layered structure and suitable valence band and conduct band position [31–33]. Moreover, previous works have demonstrated the presence of metallic Bi as a promoter has a significantly positive effect on the activity and selectivity of catalyst [34,35]. For instances, Ning and Garcia have previously reported some bismuth-modified noble metal catalysts, which

* Corresponding author.

E-mail address: rchenhku@hotmail.com (R. Chen).

exhibited improved activity and selectivity of the oxidation of glycerol to DHA due to the geometrical effect caused by the blocking of Pt surface by Bi [36,37]. Unfortunately, the essential role of bismuth promoter in improving activity and selectivity of the composited catalyst is still no fully understood, especially in photocatalysis.

Motivated by these concerns, in this work, we have developed a Bi/Bi_{3.64}Mo_{0.36}O_{6.55} heterostructure by a facile one-step solvothermal method for selective oxidation of glycerol to DHA under visible light irradiation. By utilizing the synergistic effect of metallic Bi and Bi_{3.64}Mo_{0.36}O_{6.55}, it is believed that Bi/Bi_{3.64}Mo_{0.36}O_{6.55} heterostructure might possess mild oxidation power for visible-light-driven photocatalytic selective oxidation of glycerol. To further elucidate the mechanism of the enhanced activity and selectivity over Bi/Bi_{3.64}Mo_{0.36}O_{6.55} heterostructure, the dual reaction pathways of photocatalytic glycerol oxidation was proposed, which has not been reported in previous literatures.

2. Experimental

2.1. Materials

Bismuth nitrate pentahydrate (Bi(NO₃)₃·5H₂O) and sodium hydroxide (NaOH), glycerol, 1, 2-propylene glycol, 1, 3-propylene glycol, 1, 3-dihydroxyacetone (DHA) and 1,3-diphenylisobenzofuran (DPBF) were purchased from Aladdin (Shanghai, China). Tert butyl alcohol (TBA), ammonium oxalate (C₂H₁₀N₂O₅), carbon tetrachloride (CCl₄), benzoquinone (BQ), sodium azide (NaN₃), sodium molybdate (Na₂MoO₄·2H₂O), ethanol and ethylene glycol (EG) were supplied from Sinopharm Chemical Reagent Co., Ltd. (Shanghai, China). All chemicals were used without further purification.

2.2. Preparation

In a typical procedure, 1.9403 g Bi (NO₃)₃·5H₂O and 0.4839 g Na₂MoO₄·2H₂O were dissolved into 10 mL of ethylene glycol (EG), respectively. Then the two solutions were mixed, followed by the addition of ethanol (20 mL) and sodium hydroxide aqueous solution (2 M, 6 mL). After vigorously stirring, the mixed solution was transferred into a 100 mL teflon-lined stainless steel autoclave to perform solvothermal process at 160 °C for 12 h. Subsequently, the autoclave was cooled down to room temperature naturally, and the obtained product was centrifuged and washed with ethanol for 5 times, then dried at 60 °C for characterization (**BMO-1**). Other samples (**BMO-2~BMO-4**) were prepared by using different amount of NaOH under identical experimental conditions. The experimental parameters are listed in **Table 1**.

2.3. Characterization

The composition and crystal phase were characterized by powder X-ray diffraction (XRD, Brukeraxs D8 Discover) with Cu K α radiation of 1.5406 Å. The morphology and structure were characterized by scanning electron microscope (SEM, Hitachi S4800) operating at 10.0 kV and transmission electron microscope (TEM, JEOL JSM-2010) operating at 200 kV. X-ray photo-electron spectra (XPS) were performed on a VG Multilab2000 spectrometer by using Al K α (1486.6 eV) radiation

Table 1
The experimental parameters for the preparation of **BMO** samples.

Sample	Bi source	Mo source	NaOH	Composition
BMO-1	Bi(NO ₃) ₃ ·5H ₂ O	Na ₂ MoO ₄ ·2H ₂ O	6 mL	Bi _{3.64} Mo _{0.36} O _{6.55}
BMO-2	Bi(NO ₃) ₃ ·5H ₂ O	Na ₂ MoO ₄ ·2H ₂ O	8 mL	Bi/Bi _{3.64} Mo _{0.36} O _{6.55}
BMO-3	Bi(NO ₃) ₃ ·5H ₂ O	Na ₂ MoO ₄ ·2H ₂ O	10 mL	Bi/Bi _{3.64} Mo _{0.36} O _{6.55}
BMO-4	Bi(NO ₃) ₃ ·5H ₂ O	Na ₂ MoO ₄ ·2H ₂ O	5 mL	Bi ₂ MoO ₆ /Bi _{3.64} Mo _{0.36} O _{6.55}
BMO-5^a	Bi	BMO-1	—	Bi/Bi _{3.64} Mo _{0.36} O _{6.55}

^a The experimental detail was shown in Supporting Data.

as the source. UV-vis diffuse reflectance spectra (DRS) were measured by an UV-vis spectrophotometer (HITACHI UH4150) with BaSO₄ as a reference and were converted from reflection to absorbance by the Kubelka-Munk method. Fourier transform infrared spectroscopy (FT-IR) spectra were obtained on a TENSOR 27 spectrophotometer manufactured by BRUKER Company (Germany). The steady-state fluorescence and phosphorescence spectra were obtained on a PE LS55 fluorescence spectrometer equipped with an integrating sphere (PH was recorded by accumulating 100 flash counts per point). The μ -domain time-resolved phosphorescence spectra and ns-domain time-resolved fluorescence spectra were obtained on an FLS980 fluorescence spectrometer (Edinburgh Instruments Ltd.). Photocurrent, electrochemical impedance spectroscopy and Mott-Schottky measurements were carried out on an electrochemical workstation with three-electrode (CHI-660E, China).

2.4. Evaluation of photocatalytic activity for glycerol oxidation

In a typical process, 10 mg catalyst was suspended in 3 mL of glycerol/H₂O solution (65 mmol/L). The suspension was transferred into a custom-made Pyrex glass bottle and stirred for 30 min. The reaction solution was illuminated by a 125 W Xe lamp for 4 h. After the illumination, the mixture was centrifuged at 9000 rpm for 20 min to completely remove the catalyst particles. The remaining solution was analyzed with a High performance liquid chromatograph (HPLC, Agilent 1260LC). The chemical structures of the products were confirmed by LC-MS (Agilent G6520 Q-TOF LC/MS). The conversion of glycerol and selectivity of DHA was calculated by the following equations:

$$\text{Conversion}(\%) = [(C_0 - C_{\text{GLY}})/C_0] \times 100$$

$$\text{Yield}(\%) = C_{\text{DHA}}/C_0 \times 100$$

$$\text{Selectivity}(\%) = [C_{\text{DHA}}/(C_0 - C_{\text{GLY}})] \times 100$$

where C₀, C_{GLY} and C_{DHA} was the initial concentration of glycerol, the concentration of the glycerol and DHA after photocatalytic reaction, respectively.

2.5. Reactive oxygen species (ROS) determination

Electron spin resonance (ESR) signals were examined with an electron spin resonance spectrometer (JES FA200) by using 5, 5-dimethyl-1-pyrroline-N-oxide (DMPO) and 2, 2, 6, 6-tetramethylpiperidine (TEMP) as trapping agent. The settings for the ESR spectrometer were as follows: center field (3510.00 G), microwave frequency (9.79 GHz), and power (5.05 mW). The irradiation source was a 125 W xenon lamp. Tertiary butanol, ammonium oxalate, tetrachloromethane, benzoquinone and sodium azide were added to the photocatalytic glycerol oxidation system to detect the active species in the conversion process of glycerol under identical conditions.

3. Results and discussion

Fig. 1a shows the X-ray diffraction (XRD) patterns of as-prepared samples (**BMO-1**, **BMO-2**, **BMO-3**), which displays good crystallinity. The distinct diffraction peaks of **BMO-1** correspond to pure cubic Bi_{3.64}Mo_{0.36}O_{6.55} phase (JCPDS 43-0446). However, it is found that additional diffraction peaks at 37.96, 39.62, 48.70, and 56.03 could be detected in the XRD patterns of **BMO-2** and **BMO-3**, which is well-indexed to rhombohedral Bi (JCPDS 05-0519). It is believed that the formation of metallic bismuth is owing to the weak reducing ability of EG [35]. We also found that the Bi content could be easily mediated by altering the NaOH concentration, which was verified by the stronger Bi diffraction peaks in **BMO-3** than that in **BMO-2**. Different chemical states of bismuth could be found in the deconvoluted high resolution Bi

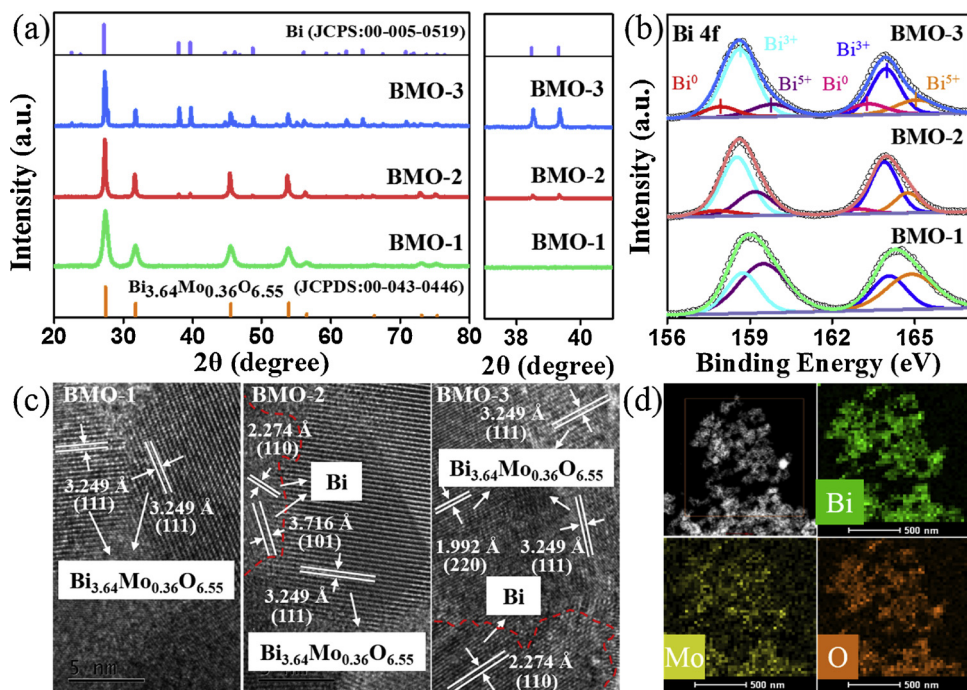


Fig. 1. Powder X-ray diffraction pattern (a), high-resolution Bi 4f XPS spectra (b), HRTEM images of BMO samples (c), and EDX mapping of BMO-2 samples (d).

4f XPS spectra of BMO samples, as shown in Fig. 1b. The binding energies at 159.7, 165.1 eV and 158.6, 164.4 eV is attributed to Bi^{5+} and Bi^{3+} in $\text{Bi}_{3.64}\text{Mo}_{0.36}\text{O}_{6.55}$, respectively [27]. And the peaks centered at 157.5 and 162.1 eV in XPS spectra of BMO-2 and BMO-3 are ascribed to metallic Bi, further demonstrating the formation of Bi/Bi_{3.64}Mo_{0.36}O_{6.55} composites [38].

All the BMO samples present uniform morphology of well-dispersed nanoparticles with the average size of 20 nm, as demonstrated by SEM and TEM images (Figure S1, Supporting Information). HRTEM images reveal the surface atomic arrangement of the as-prepared BMO nanoparticles (Fig. 1c). Two sets of characteristic lattice fringes of cubic Bi_{3.64}Mo_{0.36}O_{6.55} and metallic bismuth could be measured in HRTEM images of Bi/Bi_{3.64}Mo_{0.36}O_{6.55} heterostructures (BMO-2 and BMO-3). The d spacing of 0.3249 and 0.1992 nm are indexed to (111) and (220) crystalline planes in Bi_{3.64}Mo_{0.36}O_{6.55}, and the d spacing of 0.2274 and 0.3716 nm correspond to (110) and (101) planes of metallic Bi. Noticeably, the lattice fringes between metallic Bi and Bi_{3.64}Mo_{0.36}O_{6.55} contacted closely, indicative of the fabrication of the Bi/Bi_{3.64}Mo_{0.36}O_{6.55} heterostructure. Only one set of lattice fringes of cubic Bi_{3.64}Mo_{0.36}O_{6.55} is observed in BMO-1 sample, illustrating the pure phase of BMO-1. Moreover, the EDX mapping of BMO-2 reveal that the bismuth is well-dispersed in Bi/Bi_{3.64}Mo_{0.36}O_{6.55} without aggregation (Fig. 1d).

Consequently, the photocatalytic ability of BMO samples for glycerol oxidation to DHA under visible light are determined. The conversion and selectivity of photocatalytic oxidation of glycerol is qualitatively analyzed by HPLC measurement (Figure S2, Supporting Information). As depicted in Fig. 2, Bi/Bi_{3.64}Mo_{0.36}O_{6.55} heterostructures (BMO-2 and BMO-3) display obviously higher photocatalytic oxidation abilities than that of pure Bi_{3.64}Mo_{0.36}O_{6.55} sample (BMO-1), and BMO-2 could oxidize 42.3% of glycerol within 4 h. While the glycerol conversion over BMO-1 and BMO-3 is 28.6% and 31.9%, respectively. More importantly, Bi/Bi_{3.64}Mo_{0.36}O_{6.55} heterostructure could achieve high selectivity (97% ~ 99%) of converting glycerol to target product DHA. Compared with the reported catalysts in glycerol oxidation, Bi/Bi_{3.64}Mo_{0.36}O_{6.55} heterostructure exhibits remarkably superior photocatalytic performance for the selective oxidation of glycerol to DHA, which is summarized in Table 2. To the best of our

knowledge, the simultaneously realization of high selectivity and high yield of glycerol oxidation to DHA has rarely been reported.

To understand the highly selective oxidation ability of Bi/Bi_{3.64}Mo_{0.36}O_{6.55} heterostructure in the glycerol oxidation, the photocatalytic oxidation of glycerol over BMO samples are also performed in different atmospheres (Fig. 3a and b). It is found that the DHA yield is highly related to the involved O₂ in the glycerol oxidation, illustrating that the oxidation of glycerol involves in a photocatalytic oxygen activation process. Thus, electron spin resonance (ESR) measurement is used to determine the possible produced reactive oxygen species (ROS). As illustrated in Fig. 3c, both $\cdot\text{O}_2^-$ and $\cdot\text{O}_2$ could be generated in the presence of BMO samples upon light irradiation, and negligible $\cdot\text{OH}$ signals could be observed in the ESR spectra of all BMO samples. Specifically, BMO-2 with highest photocatalytic ability of glycerol oxidation to DHA could yield highest $\cdot\text{O}_2$ amount under identical conditions. While BMO-1 possesses highest ability of generating $\cdot\text{O}_2^-$ among BMO samples. As we known, $\cdot\text{O}_2$ is one of the highly reactive oxygen species, which could act as a mild oxidant for selective oxidation [49–51]. Hence, it is believed that the highly selective oxidation ability of BMO-2 for glycerol to DHA is closely related to the mass-produced $\cdot\text{O}_2$. Therefore, the scavenge experiments are carried out to clarify the contribution of $\cdot\text{O}_2$ in the selective oxidation of glycerol to DHA. As shown in Figure S3 (Supporting Information), the pumping of N₂ obviously inhibits the production of DHA, illustrating the involvements of reactive oxygen species in the glycerol oxidation. The addition of TBA ($\cdot\text{OH}$ scavenger) and BQ ($\cdot\text{O}_2^-$ scavenger) have slight influence on the DHA yield. However, the DHA yield decreases dramatically in the presence of Na₃ ($\cdot\text{O}_2$ scavenger), suggesting that $\cdot\text{O}_2$ was the dominating reactive species for the photocatalytic oxidation of glycerol to DHA.

Due to the stronger oxidation ability of $\cdot\text{O}_2^-$ than that of $\cdot\text{O}_2$, the peroxidation of glycerol usually would occur in the presence of $\cdot\text{O}_2^-$, which leads to the generation of other organic products, instead of DHA. Therefore, the little production of $\cdot\text{O}_2^-$ over BMO-2 had no influence on the selective oxidation of glycerol to DHA. To verify this, Bi₂MoO₆/Bi_{3.64}Mo_{0.36}O_{6.55} heterostructure (BMO-4) with more generated $\cdot\text{O}_2^-$ radicals is prepared (Figure S4, Supporting information). Compared with BMO-2, the dominated $\cdot\text{O}_2^-$ produced in BMO-4 would

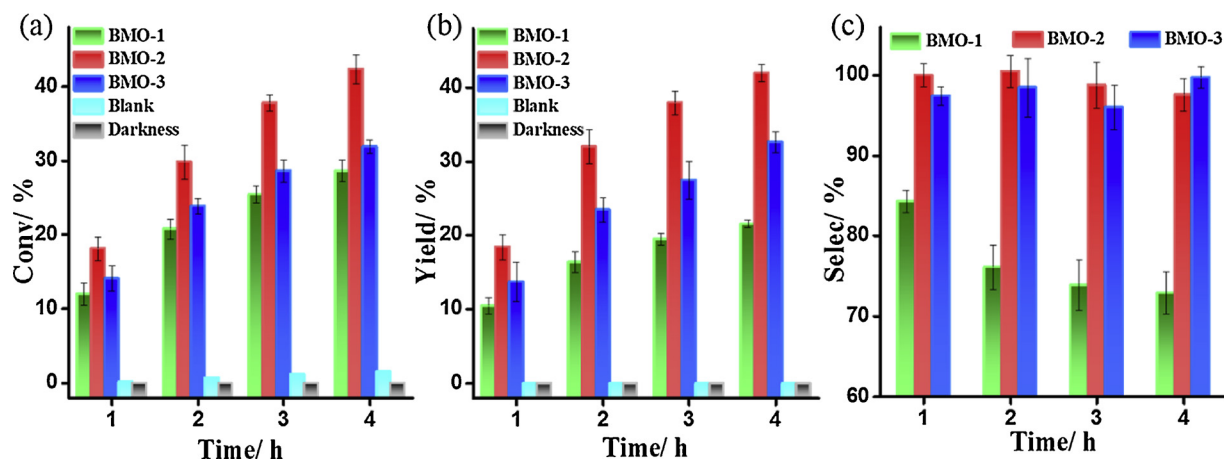


Fig. 2. The conversion (a), yield (b) and selectivity of photocatalytic glycerol oxidation to DHA (c) under visible light irradiation over BMO samples.

over-oxidize glycerol to glycolic acid, instead of DHA, under identical photocatalytic conditions, as shown in Figure S5 (Supporting Information). It further illustrate that the highest DHA yield of **BMO-2** in the photocatalytic oxidation of glycerol is ascribed to the large production of $^1\text{O}_2$.

To figure out the enhanced $^1\text{O}_2$ generation in Bi/Bi_{3.64}Mo_{0.36}O_{6.55} heterostructure, photoluminescence experiments are performed to elucidate the energy transfer process in the production of $^1\text{O}_2$, which involves the spin-flip of triplet excitons [52,53]. The mean lifetimes calculated from the kinetics of the time-resolved fluorescence (PF) spectra is 3.13 and 2.57 ns for **BMO-1** and **BMO-2**, respectively (Fig. 4a). It indicates a more effective electron excitation from singlet to triplet in the **BMO-2** sample. And the stronger phosphorescence (PH) intensity of **BMO-2** also demonstrates its better photoactivation of triplet excitons than that of **BMO-1** (Fig. 4b). The steady-state fluorescence (PF) and phosphorescence (PH) spectra reveal that the energy gap between the singlet and triplet state (ΔE_{ST}) of **BMO-2** (0.183 eV) is much smaller than that of **BMO-1** (0.314 eV) (Fig. 4c). On the other hand, the time-resolved phosphorescence (PH) spectra illustrate the

longer average PH lifetime of **BMO-1** (144.60 μs) than that of **BMO-2** (68.85 μs), which implies a stronger spin-orbit coupling (SOC) of **BMO-2** (Fig. 4d). Based on the Franck-Condon principle, the energy transfer rate is mainly determined by the energy gap (ΔE_{ST}) and spin-orbit coupling (SOC) between singlet and triplet states [54]. Therefore, the reduced ΔE_{ST} and enhanced SOC of **BMO-2** facilitates the energy transfer process and favors the efficient $^1\text{O}_2$ generation. It is also found that the oxygen vacancy in **BMO** sample plays significant role in the generation of $^1\text{O}_2$. As shown in Fig. 4e, the solid electron paramagnetic resonance (EPR) signals with g-value of 2.00 are observed in the EPR spectra of **BMO-2**, which is attributed to the Zeeman Effect of single electron trapped by oxygen vacancies. The high resolution O 1 s XPS spectrum of **BMO-2** sample (Fig. 4f) also reveals an obvious shoulder peak located at 532.1 eV, which is associated with O²⁻ ions in the oxygen deficient regions (ODR) [55]. To further confirm the function of oxygen vacancy in the generation of $^1\text{O}_2$, Bi/Bi_{3.64}Mo_{0.36}O_{6.55} nanoparticles without oxygen vacancies (**BMO-5**) was also prepared and characterized (Figure S6, Supporting Information). The $^1\text{O}_2$ production ability of **BMO-5** was determined by using the chemical trapping probe

Table 2
Summary of the results of catalytic oxidation of glycerol.

Entry	Catalyst	Catal. Amt.	GLY Conc.	Time /h	Oxidation method	Temp./°C	Conv. /%	Selectivity / %					Ref.	
								GAD	DHA	GCA	LA	GCOA		
1	Bi/Bi _{3.64} Mo _{0.36} O _{6.55}	3.3*	6 a *	4	125 W Xe lamp	25	42.3	—	97.6	—	—	—	This work	
2	Degussa P25	0.2*	9.2 a *	24.5	125 W Hg lamp	25	35	7	4	—	—	—	[15]	
3	TiO ₂	1*	1.84 a *	4	300 W Xe lamp	80	20	—	—	—	49	—	[29]	
4	ZnO	2.5*	0.276 a *	1	125 W Hg lamp	40	36.2	39.3	17.7	—	—	—	[39]	
5	TiO ₂ -H ₂ O ₂	3*	2.76 a *	8	120 W Hg lamp	—	71.42	—	0.39	19.61	—	—	[14]	
6	TiSi ₂	10*	100 a *	12	300 W Xe lamp	65	97.6	—	—	100	—	—	[40]	
7	Na ₄ W ₁₀ O ₃₂ /SiO ₂	8*	0.92 a *	2	> 290 nm	25	16	59.4	5.6	5.3	—	—	[25]	
8	7.5 wt.% Au/TiO ₂	1*	4.6 a *	15	> 420 nm	90	48	8	50	—	—	5	[30]	
9	Bi ₂ WO ₆	5.3*	0.046 a *	12	> 420 nm	25	90	—	93	—	—	—	[26]	
10	5 wt.% Pd/TiO ₂	25*	46 a *	18	450 W Xe lamp	25	19	17	9	—	—	30	[3]	
11	0.5% Au/TiO ₂	1:40‡	55.2 a *	4	Metal catalysis	60	54	—	—	30	—	40	[42]	
12	2 wt.% Pd-Bi/C	2.5*	50 a *	4	Metal catalysis	200	1.8	33.1	54.1	10.1	—	—	[43]	
13	2 wt.% AuPd/TiO ₂	2500‡	46 c *	4	Metal catalysis	140	25.5	—	8.3	5.4	—	2.4	[44]	
14	0.64 wt.% Pt/HT	2500‡	9.2 a *	24	Metal catalysis	90	54	74	—	—	—	—	[45]	
15	AuPt(1:3)/MgO	500‡	27.6 a *	24	Metal catalysis	25	29.7	—	—	66.7	—	11.5	[46]	
16	1%Bi-5%Pt charcoal	5*	100 a *	4	Metal catalysis	50	30	—	20	—	—	—	[24]	
17	NCNTs800	5ƒ	1380 b *	6	Metal catalysis	60	8.3	—	73.8	—	—	—	6.5	[5]
18	[Cp*Ir(Me) ₂ Cl]BF ₄	143‡	1 a †	15	Metal catalysis	115	4.5	—	—	—	95	—	[21]	
19	[Ir(COD)(Me) ₂]BF ₄	500‡	Neat a	40	Metal catalysis	115	50	—	—	—	0.98	—	0.01	[21]
20	TEMPO	0.0075#	4.6 d *	20	Electro-catalysis	—	25	—	100	—	—	—	[23]	
21	PtSb/C	—	9.2 a *	10	Electro-catalysis	60	95.8	—	35.4	—	—	—	[47]	
22	C. pasteurianum	—	75~90 *	25	Microbial fermentation	—	77.4	—	—	25	—	—	[48]	

Reaction conditions: ^a H₂O ^b TPBH (70% in water) ^c AlCl₃ (10 mmol L⁻¹ in water). ^d Na₂CO₃ (0.2 M) Unit: * g/L. ‡ glycerol/metal (mol/mol). ƒ glycerol/catalyst (wt:wt). † glycerol/water (V: V). # mol/L.

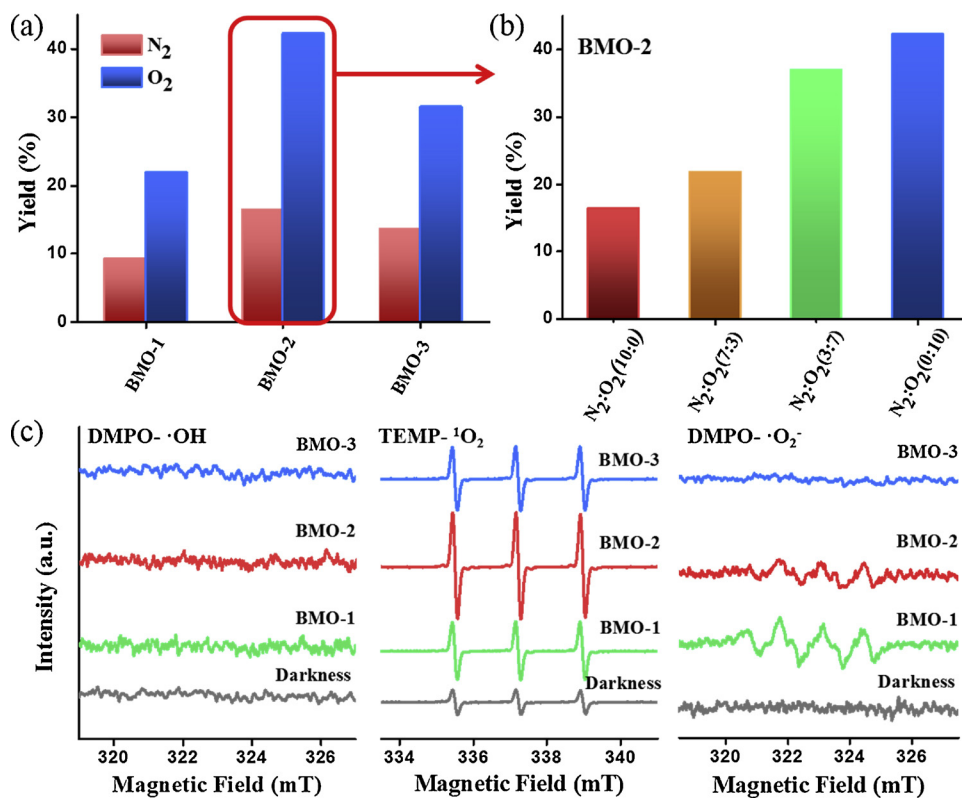


Fig. 3. The DHA yield of photocatalytic glycerol oxidation over **BMO-2** in the presence of saturated N_2 and O_2 atmosphere (a), different proportion of N_2/O_2 gas mixture (b) and ESR spectra of DMPO-·OH, TEMP-· O_2 and DMPO-· O_2^- of **BMO** samples (c).

(DPBF), compared with **BMO-2** and **BMO-1**. (Figure S7, Supporting Information). The decay rate of DPBF in the presence of **BMO-2** was significantly larger than that of **BMO-5**, which displays equivalent 1O_2 production ability with **BMO-1**. It illustrates that the generation of oxygen vacancies in **BMO-2** sample promoted the generation of 1O_2 . In the reported literatures, oxygen vacancies could form oxygen vacancy states lying close to the conduction band of the photocatalyst, which were likely to affect the energy gap in the sample [56]. Hence, it is proposed that the oxygen vacancies in **BMO-2** sample could form a new energy state below the conduction band to decrease the energy gap, thus enhancing the triplet-exciton yield by synergistically promoting intersystem-crossing and reducing the singlet-triplet energy gap of the matrix, and facilitating the 1O_2 generation through the energy transfer process. This is also in accordance with our previously reported work [51].

In this work, although it is found that the photogenerated electrons is extremely important for the generation of ROS in the photocatalytic oxidation of glycerol, the photogenerated holes also greatly contribute to the selective oxidation of glycerol to DHA. As confirmed by the scavenge experiments, the DHA yield dramatically decreases from 42% to 25% over **BMO-2** with the addition of AO (hole scavenger) (Figure S8, Supporting Information), implying that the photogenerated holes also contribute to the selective oxidation of glycerol to DHA. It is well known that the generation of metal-semiconductor junction might improve the migration efficiency of photogenerated carriers and suppress the recombination of hole-electron effectively, which would highly affect the hole generation process. Hence, electrochemical impedance spectroscopy (EIS) was performed to investigate the separation efficiency of the photogenerated carriers. Compared with the pure $Bi_{3.64}Mo_{0.36}O_{6.55}$ (**BMO-1**), **BMO-2** presents the smaller arc radius, suggesting the superior separation efficiency of the photoinduced electron-hole and the charge transfer (Figure S9a, Supporting Information). The transient photocurrent response of **BMO** samples also reveals that **BMO-2** enhances the photocurrent density significantly,

compared with **BMO-1** (Figure S9b, Supplementary Data). It illustrates that the metallic Bi could promote the separation of photogenerated carriers on $Bi_{3.64}Mo_{0.36}O_{6.55}$ and facilitate the generation of hole. However, the photocurrent density of **BMO-3** decreases due to the shielding effect of the excessive Bi nanocrystals on the surface [35,38,57].

The potential of photogenerated holes in $Bi/Bi_{3.64}Mo_{0.36}O_{6.55}$ heterostructure is no doubt significant in the selective oxidation of glycerol to DHA which was determined by Mott-Schottky plots and valence band XPS spectra (Fig. 5a). The calculated band potential of $Bi_{3.64}Mo_{0.36}O_{6.55}$ is -0.33 and 2.10 eV vs NHE for the conduction and valence band, respectively. Moreover, the redox potentials of glycerol and DHA are evaluated by the cyclic voltammetry in different concentrations (1 and 2 mM). As illustrated in Fig. 5b, the redox potential is estimated to be 1.78 and 2.02 eV vs Hg/Hg_2Cl_2 (i.e., 2.02 and 2.26 eV vs NHE) for glycerol and DHA, respectively. Theoretically, the photogenerated holes could oxidize glycerol to produce glyceraldehyde or DHA via two pathway. The oxidation of primary hydroxyl group of glycerol results in the production of glyceraldehyde, and the oxidation of secondary hydroxyl group is more favorable for the generation of DHA. However, in this work, only DHA was obtained. Therefore, owing to the geometrical effect, the coordination of glycerol with the surface of catalyst is critical in the selectivity of the oxidation of glycerol [58,59]. To investigate the influence of the combination of glycerol on the surface of the $Bi/Bi_{3.64}Mo_{0.36}O_{6.55}$ during the selective oxidation process, FT-IR spectra of **BMO** samples before and after glycerol absorption are recorded.

As shown in Fig. 5c, the intensity of the absorption peak corresponded to glycerol (994, 1043, 1110, 2882 and 2936 cm^{-1}) from $Bi/Bi_{3.64}Mo_{0.36}O_{6.55}$ heterostructure (**BMO-2** and **BMO-3**) is remarkably stronger than that of pure $Bi_{3.64}Mo_{0.36}O_{6.55}$ (**BMO-1**) after adsorption-desorption equilibrium in glycerol solution. Moreover, the absorbed glycerol increases with the increase of Bi content in $Bi/Bi_{3.64}Mo_{0.36}O_{6.55}$ heterostructure, illustrating that bismuth function as adsorption sites to facilitate the surface complexation with glycerol. To

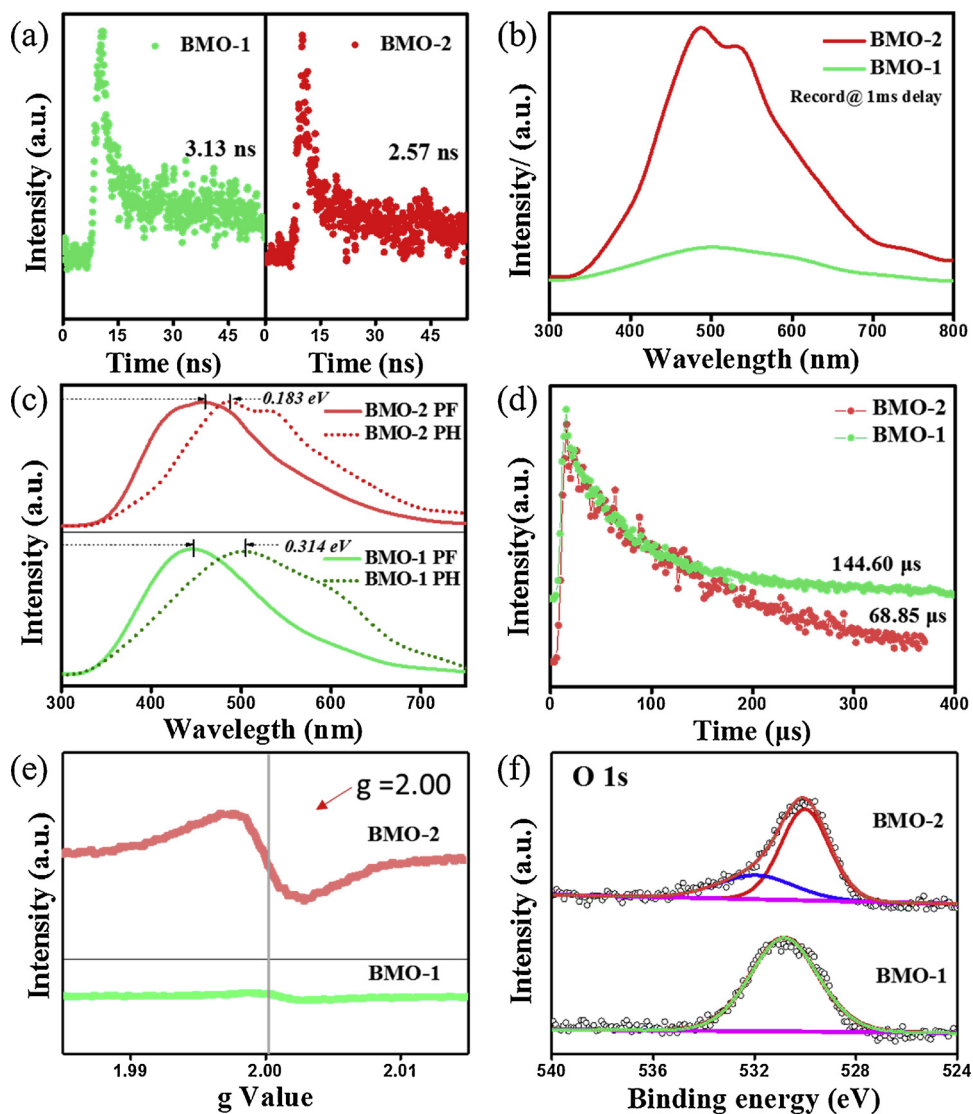


Fig. 4. Time-resolved PF kinetics (excitation at 275 nm) (a), PH spectra (delay time 1 ms, excitation at 275 nm) (b), the normalized steady-state PF and PH spectra (c), time-resolved PH kinetics (excitation at 275 nm) (d), EPR spectra (e) and High-resolution O 1 s XPS spectra (f) of BMO-1 and BMO-2 samples.

further understand the binding mode of Bi/Bi_{3.64}Mo_{0.36}O_{6.55} with glycerol, 1, 2-propylene and 1, 3-propylene glycol are instead of glycerol to perform the FT-IR spectra of BMO samples after adsorption, respectively. It is observed that the peak intensity of adsorbed 1, 2-propylene glycol is proportional to the bismuth content. However, the content of Bi in Bi/Bi_{3.64}Mo_{0.36}O_{6.55} heterostructure exhibits negligible influence on the adsorption of 1, 3-propylene glycol (Figure S10, Supplementary Information). Fig. 5d shows that the correlation between the Bi content and the relative polyol adsorption amount, and the calculated correlation coefficient is 0.9466, 0.9353 and 0.3828, respectively. Hence, the interaction mode of the glycerol and its derivatives with Bi/Bi_{3.64}Mo_{0.36}O_{6.55} is proposed in Fig. 5e. It illustrates that the metallic Bi in Bi/Bi_{3.64}Mo_{0.36}O_{6.55} facilitates the complexation of bismuth with ortho-hydroxyl in glycerol, which is beneficial for the selective oxidation of glycerol to produce DHA. Based on the results, it is evident that Bi/Bi_{3.64}Mo_{0.36}O_{6.55} could selectively oxidize glycerol to DHA via dual reaction pathways, which is illustrated in Scheme 1.

4. Conclusions

In summary, the Bi/Bi_{3.64}Mo_{0.36}O_{6.55} heterostructure have been successfully synthesized via a facile solvothermal method, which

displays remarkable photocatalytic ability for selective glycerol oxidation to DHA under visible light irradiation. Moreover, the deep understanding of the high selectivity of Bi/Bi_{3.64}Mo_{0.36}O_{6.55} heterostructure for photocatalytic oxidation of glycerol is discussed. The reduced energy gap (ΔE_{ST}), enhanced spin-orbit coupling (SOC) and the presence of oxygen vacancies in Bi/Bi_{3.64}Mo_{0.36}O_{6.55} heterostructure favors the generation of dominated $^1\text{O}_2$ reactive oxygen species. On the other hand, the metallic bismuth promotes the separation of photo-generated carries and the generation of holes with efficient redox potential for glycerol oxidation, and the coordination of bismuth with ortho-hydroxyl in glycerol facilitates the selective oxidation to DHA. The dual-pathway reaction process greatly promotes the selective oxidation of glycerol to DHA simultaneously. This work paves the way for the development of highly efficient heterostructured photocatalysts for selective oxidation.

Notes

The authors declare no competing financial interest.

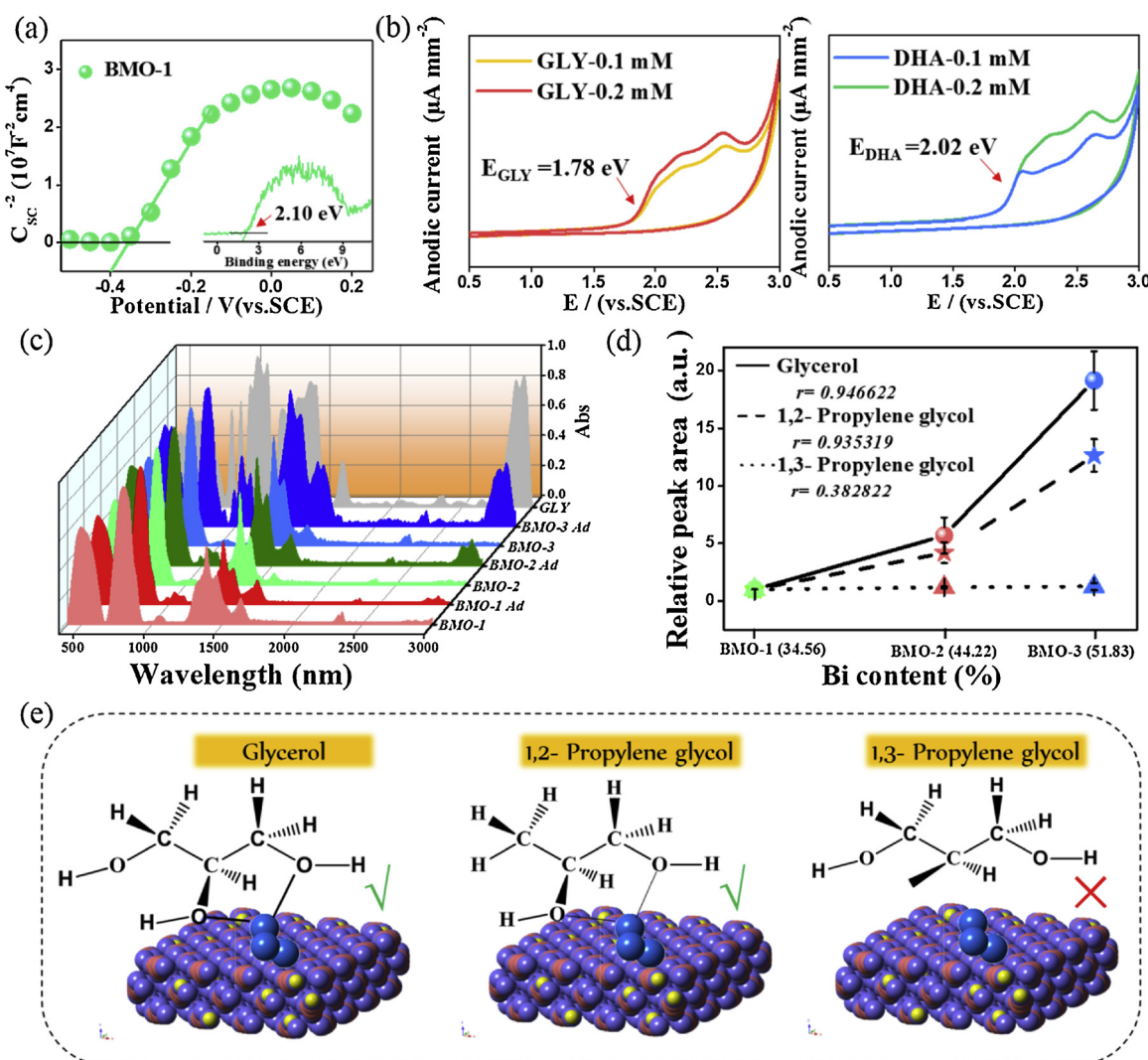
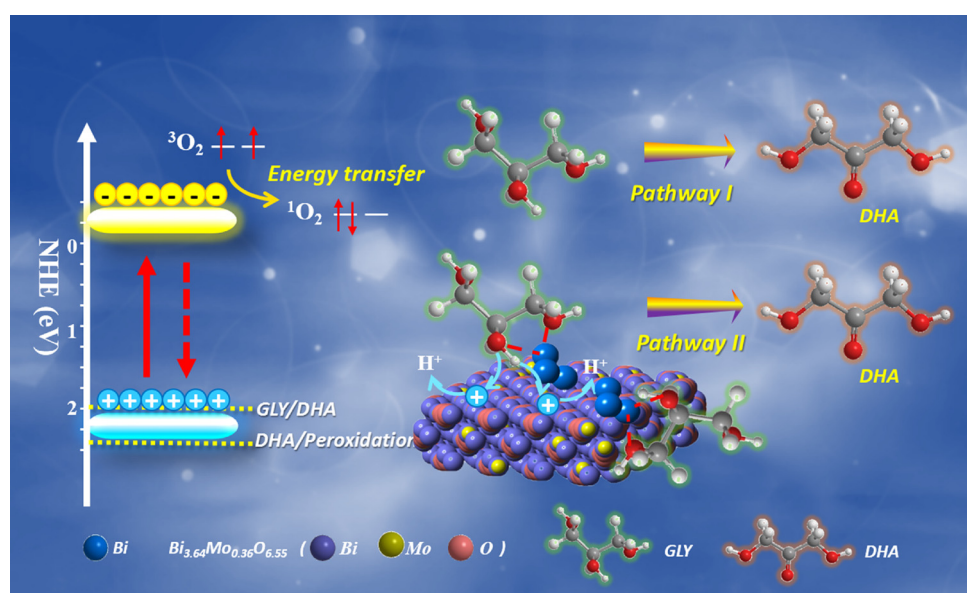


Fig. 5. Mott-Schottky plots and band XPS spectra (inset) of BMO-1 (a), the cyclic voltammogram of glycerol and DHA with different concentrations (b), FT-IR spectra of glycerol and BMO samples before and after glycerol adsorption (c), the correlation between the Bi content and relative polyol adsorption amount (d), and schematic illustration of the proposed of the glycerol intermediate with BMO samples (e).



Scheme 1. Proposed photocatalytic reaction pathways of selective oxidation of glycerol to DHA over $\text{Bi}/\text{Bi}_{3.64}\text{Mo}_{0.36}\text{O}_{6.55}$ heterostructure.

Acknowledgements

This work was supported by the National Natural Science Foundation of China (21671153 and 21471121), Department of Education of Hubei Province under the Project of Science and Technology Innovation Team of Outstanding Young and Middle-aged Scientists (T201606) and Open Research Fund of the State Key Laboratory of Inorganic Synthesis and Preparative Chemistry (Jilin University, 2017-02).

Appendix A. Supplementary data

Supplementary material related to this article can be found, in the online version, at doi:<https://doi.org/10.1016/j.apcatb.2018.11.047>.

References

- [1] L. Wang, F.-S. Xiao, Nanoporous catalysts for biomass conversion, *Green. Chem.* 17 (2015) 24–39.
- [2] C.H. Zhou, H. Zhao, D.S. Tong, L.M. Wu, W.H. Yu, Recent advances in catalytic conversion of glycerol, *Catal. Rev.* 55 (2013) 369–453.
- [3] M. Pagliaro, R. Ciriminna, H. Kimura, M. Rossi, C. Della Pina, From glycerol to value-added products, *Angew. Chem. Int. Ed.* 46 (2007) 4434–4440.
- [4] H. Tan, O.E. Tall, Z. Liu, N. Wei, T. Yapici, T. Zhan, M.N. Hedhill, Y. Han, Selective oxidation of glycerol to glyceric acid in base-free aqueous solution at room temperature catalyzed by platinum supported on carbon activated with potassium hydroxide, *ChemCatChem* 8 (2016) 1699–1707.
- [5] N. Gupta, O. Khavryuchenko, A. Villa, D. Su, Metal-free oxidation of glycerol over nitrogen-containing carbon nanotubes, *ChemSusChem* 10 (2017) 3030–3034.
- [6] C. Chan-Thaw, S. Campisi, D. Wang, L. Prati, A. Villa, Selective oxidation of raw glycerol using supported AuPd nanoparticles, *Catalysts* 5 (2015) 131–144.
- [7] L.S. Ribeiro, E.G. Rodrigues, J.J. Delgado, X. Chen, M.F.R. Pereira, J.J.M. Órfão, Pd, Pt, and Pt–Cu catalysts supported on carbon nanotube (CNT) for the selective oxidation of glycerol in alkaline and base-free conditions, *Ind. Eng. Chem. Res.* 55 (2016) 8548–8556.
- [8] X. Li, Y. Zhang, Oxidative dehydration of glycerol to acrylic acid over vanadium-substituted cesium salts of keggin-type heteropolyacids, *ACS Catal.* 6 (2016) 2785–2791.
- [9] D. Liang, J. Gao, J. Wang, P. Chen, Z. Hou, X. Zheng, Selective oxidation of glycerol in a base-free aqueous solution over different sized Pt catalysts, *Catal. Commun.* 10 (2009) 1586–1590.
- [10] R. Nie, D. Liang, L. Shen, J. Gao, P. Chen, Z. Hou, Selective oxidation of glycerol with oxygen in base-free solution over MWCNTs supported PtSb alloy nanoparticles, *Appl. Catal. B: Environ.* 127 (2012) 212–220.
- [11] D. Liang, J. Gao, H. Sun, P. Chen, Z. Hou, X. Zheng, Selective oxidation of glycerol with oxygen in a base-free aqueous solution over MWNTs supported Pt catalysts, *Appl. Catal. B: Environ.* 106 (2011) 423–432.
- [12] G.M. Lari, C. Mondelli, J. Pérez-Ramírez, Gas-phase oxidation of glycerol to dihydroxyacetone over tailored iron zeolites, *ACS Catal.* 5 (2015) 1453–1461.
- [13] R.M. Painter, D.M. Pearson, R.M. Waymouth, Selective catalytic oxidation of glycerol to dihydroxyacetone, *Angew. Chem. Int. Ed.* 49 (2010) 9456–9459.
- [14] T. Jedsukontorn, V. Meeyoo, N. Saito, M. Hunsom, Route of glycerol conversion and product generation via TiO₂-induced photocatalytic oxidation in the presence of H₂O₂, *Chem. Eng. J.* 281 (2015) 252–264.
- [15] V. Augugliaro, H.A.H. El Nazer, V. Loddo, A. Mele, G. Palmisano, L. Palmisano, S. Yurdakal, Partial photocatalytic oxidation of glycerol in TiO₂ water suspensions, *Catal. Today* 151 (2010) 21–28.
- [16] R. Bauer, N. Katsikis, S. Varga, D. Hekmat, Study of the inhibitory effect of the product dihydroxyacetone on gluconobacter oxydans in a semi-continuous two-stage repeated-fed-batch process, *Bioprocess. Biosyst. Eng.* 28 (2005) 37–43.
- [17] Z. Chi, D. Pyle, Z. Wen, C. Frear, S. Chen, A laboratory study of producing docosahexaenoic acid from biodiesel-waste glycerol by microalgal fermentation, *Process Biochem.* 42 (2007) 1537–1545.
- [18] N.A. Romero, D.A. Nicewicz, Organic photoredox catalysis, *Chem. Rev.* 116 (2016) 10075–10166.
- [19] F. Raza, J.H. Park, H.-R. Lee, H.-I. Kim, S.-J. Jeon, J.-H. Kim, Visible-light-driven oxidative coupling reactions of amines by photoactive WS₂ nanosheets, *ACS Catal.* 6 (2016) 2754–2759.
- [20] M. Yuan, F. Tian, G. Li, H. Zhao, Y. Liu, R. Chen, Fe(III)-modified BiOBr hierarchitectures for improved photocatalytic benzyl alcohol oxidation and organic pollutants degradation, *Ind. Eng. Chem. Res.* 56 (2017) 5935–5943.
- [21] L.S. Sharninghausen, J. Campos, M.G. Manas, R.H. Crabtree, Efficient selective and atom economic catalytic conversion of glycerol to lactic acid, *Nat. Commun.* 5 (2014) 5084.
- [22] Z. Lu, I. Demianets, R. Hamze, N.J. Terrile, T.J. Williams, A prolific catalyst for selective conversion of neat glycerol to lactic acid, *ACS Catal.* 6 (2016) 2014–2017.
- [23] R. Ciriminna, G. Palmisano, C.D. Pina, M. Rossi, M. Pagliaro, One-pot electrocatalytic oxidation of glycerol to DHA, *Tetrahedron Lett.* 47 (2006) 6993–6995.
- [24] C.H. Zhou, J.N. Beltramini, Y.X. Fan, G.Q. Lu, Chemosselective catalytic conversion of glycerol as a biorenewable source to valuable commodity chemicals, *Chem. Soc. Rev.* 37 (2008) 527–549.
- [25] A. Molinari, A. Maldotti, A. Bratovic, G. Magnacca, Photocatalytic properties of sodium decatungstate supported on sol-gel silica in the oxidation of glycerol, *Catal. Today* 206 (2013) 46–52.
- [26] Y. Zhang, N. Zhang, Z.-R. Tang, Y.-J. Xu, Identification of Bi₂WO₆ as a highly selective visible-light photocatalyst toward oxidation of glycerol to dihydroxyacetone in water, *Chem. Sci.* 4 (2013) 1820–1824.
- [27] L.N. Song, L. Chen, J. He, P. Chen, H.K. Zeng, C. Au, S.F. Yin, First synthesis of Bi self-doped Bi₂MoO₆·Bi₂Mo₃O₁₂ composite and its excellent photocatalytic performance for selective oxidation of aromatic alkanes under visible light irradiation, *Chem. Commun.* 53 (2017) 6480–6483.
- [28] B. Zhang, J. Li, Y. Gao, R. Chong, Z. Wang, L. Guo, X. Zhang, C. Li, To boost photocatalytic activity in selective oxidation of alcohols on ultrathin Bi₂MoO₆ nanoplates with Pt nanoparticles as cocatalyst, *J. Catal.* 345 (2017) 96–103.
- [29] R. Chong, J. Li, X. Zhou, Y. Ma, J. Yang, L. Huang, H. Han, F. Zhang, C. Li, Selective photocatalytic conversion of glycerol to hydroxyacetalddehyde in aqueous solution on facet tuned TiO₂-based catalysts, *Chem. Commun.* 50 (2014) 165–167.
- [30] G. Dodekatos, H. Tuysuz, Plasmonic Au/TiO₂ nanostructures for glycerol oxidation, *Catal. Sci. Technol.* 6 (2016) 7307–7315.
- [31] Z. Dai, F. Qin, H. Zhao, J. Ding, Y. Liu, R. Chen, Crystal defect engineering of aurivillius Bi₂MoO₆ by Ce doping for increased reactive species production in photocatalysis, *ACS Catal.* 6 (2016) 3180–3192.
- [32] Z. Dai, F. Qin, H. Zhao, F. Tian, Y. Liu, R. Chen, Time-dependent evolution of the Bi_{3.64}Mo_{0.36}O_{6.55}·Bi₂MoO₆ heterostructure for enhanced photocatalytic activity via the interfacial hole migration, *Nanoscale* 7 (2015) 11991–11999.
- [33] J. Xiong, G. Cheng, F. Qin, R. Wang, H. Sun, R. Chen, Tunable BiOCl hierarchical nanostructures for high-efficient photocatalysis under visible light irradiation, *Chem. Eng. J.* 220 (2013) 228–236.
- [34] Y. Xiao, J. Greeley, A. Varma, Z.-J. Zhao, G. Xiao, An experimental and theoretical study of glycerol oxidation to 1,3-dihydroxyacetone over bimetallic Pt-Bi catalysts, *AICHE J.* 63 (2016) 705–715.
- [35] F. Tian, H. Zhao, G. Li, Z. Dai, Y. Liu, R. Chen, Modification with metallic bismuth as efficient strategy for the promotion of photocatalysis: the case of bismuth phosphate, *ChemSusChem* 9 (2016) 1579–1585.
- [36] X. Ning, Y. Li, H. Yu, F. Peng, H. Wang, Y. Yang, Promoting role of bismuth and antimony on Pt catalysts for the selective oxidation of glycerol to dihydroxyacetone, *J. Catal.* 335 (2016) 95–104.
- [37] A.C. Garcia, Y.Y. Birdja, G. Tremeliosi-Filho, M.T.M. Koper, Glycerol electro-oxidation on bismuth-modified platinum single crystals, *J. Catal.* 346 (2017) 117–124.
- [38] Y. Ma, Y. Jia, L. Wang, M. Yang, Y. Bi, Y. Qi, Efficient charge separation between Bi and Bi₂MoO₆ for photoelectrochemical properties, *Chemistry* 22 (2016) 5844–5848.
- [39] A. Natanael, André R. Hermes, AmiseS. Corsetti, M.A. Pacheco, Lansarin, Photocatalytic oxidation of glycerol over ZnO: systematic evaluation of reaction parameters, *J. Adv. Oxid. Technol.* 18 (2015) 315–321.
- [40] N. Kondamudi, M. Misra, S. Banerjee, S. Mohapatra, S. Mohapatra, Simultaneous production of glyceric acid and hydrogen from the photooxidation of crude glycerol using TiSi₂, *Appl. Catal. B: Environ.* 126 (2012) 180–185.
- [41] B. Zhou, J. Song, H. Zhou, L. Wu, T. Wu, Z. Liu, B. Han, Light-driven integration of the reduction of nitrobenzene to aniline and the transformation of glycerol into valuable chemicals in water, *RSC Adv.* 5 (2015) 36347–36352.
- [42] C. D'Agostino, G. Brett, G. Divitini, C. Ducati, G.J. Hutchings, M.D. Mantle, L.F. Gladden, Increased affinity of small gold particles for glycerol oxidation over Au/TiO₂ probed by NMR relaxation methods, *ACS Catal.* 7 (2017) 4235–4241.
- [43] S. Hirasawa, H. Watanabe, T. Kizuka, Y. Nakagawa, K. Tomishige, Performance, structure and mechanism of Pd–Ag alloy catalyst for selective oxidation of glycerol to dihydroxyacetone, *J. Catal.* 300 (2013) 205–216.
- [44] J. Xu, H. Zhang, Y. Zhao, B. Yu, S. Chen, Y. Li, L. Hao, Z. Liu, Selective oxidation of glycerol to lactic acid under acidic conditions using AuPd/TiO₂ catalyst, *Green Chem.* 15 (2013) 1520–1525.
- [45] A. Tsuji, K.T. Rao, S. Nishimura, A. Takagaki, K. Ebitani, Selective oxidation of glycerol by using a hydrotalcite-supported platinum catalyst under atmospheric oxygen pressure in water, *ChemSusChem* 4 (2011) 542–548.
- [46] G.L. Brett, Q. He, C. Hammond, P.J. Miedziak, N. Dimitratos, M. Sankar, A.A. Herzing, M. Conte, J.A. Lopez-Sánchez, C.J. Kiely, D.W. Knight, S.H. Taylor, G.J. Hutchings, Selective oxidation of glycerol by highly active bimetallic catalysts at ambient temperature under base-free conditions, *Angew. Chem. Int. Ed.* 50 (2011) 10136–10139.
- [47] S. Lee, H.J. Kim, E.J. Lim, Y. Kim, Y. Noh, G.W. Huber, W.B. Kim, Highly selective transformation of glycerol to dihydroxyacetone without using oxidants by PtSb/C-catalyzed electrooxidation process, *Green Chem.* 18 (2016) 2877–2887.
- [48] D.T. Johnson, K.A. Taconi, The glycerin glut: options for the value-added conversion of crude glycerol resulting from biodiesel production, *Environ. Prog.* 26 (2007) 338–348.
- [49] A.A. Ghogare, A. Greer, Using singlet oxygen to synthesize natural products and drugs, *Chem. Rev.* 116 (2016) 9994–10034.
- [50] Y.Z. Chen, Z.U. Wang, H. Wang, J. Lu, S.H. Yu, H.L. Jiang, Singlet oxygen-engaged selective photo-oxidation over Pt nanocrystals/porphyrinic MOF: the roles of photothermal effect and Pt electronic state, *J. Am. Chem. Soc.* 139 (2017) 2035–2044.
- [51] J. Ding, Z. Dai, F. Tian, B. Zhou, B. Zhao, H. Zhao, Z. Chen, Y. Liu, R. Chen, Generation of defect clusters for ¹O₂ production for molecular oxygen activation in photocatalysis, *J. Mater. Chem. A* 5 (2017) 23453–23459.
- [52] H. Wang, S. Chen, D. Yong, X. Zhang, S. Li, W. Shao, X. Sun, B. Pan, Y. Xie, Giant electron-hole interactions in confined layered structures for molecular oxygen activation, *J. Am. Chem. Soc.* 139 (2017) 4737–4742.
- [53] H. Wang, X. Sun, D. Li, X. Zhang, S. Chen, W. Shao, Y. Tian, Y. Xie, Boosting hot-

electron generation: exciton dissociation at the order-disorder interfaces in polymeric photocatalysts, *J. Am. Chem. Soc.* 139 (2017) 2468–2473.

[54] H. Wang, S. Jiang, S. Chen, D. Li, X. Zhang, W. Shao, X. Sun, J. Xie, Z. Zhao, Q. Zhang, Y. Tian, Y. Xie, Enhanced singlet oxygen generation in oxidized graphitic carbon nitride for organic synthesis, *Adv. Mater.* 28 (2016) 6940–6945.

[55] J. Ding, Z. Dai, F. Qin, H. Zhao, S. Zhao, R. Chen, Z-scheme $\text{BiO}_{1-x}\text{Br}/\text{Bi}_2\text{O}_2\text{CO}_3$ photocatalyst with rich oxygen vacancy as electron mediator for highly efficient degradation of antibiotics, *Appl. Catal. B: Environ.* 205 (2017) 281–291.

[56] H. Li, F. Qin, Z. Yang, X. Cui, J. Wang, L. Zhang, New reaction pathway induced by plasmon for selective benzyl alcohol oxidation on BiOCl possessing oxygen vacancies, *J. Am. Chem. Soc.* 139 (2017) 3513–3521.

[57] M. Jin, S. Lu, L. Ma, M. Gan, One-step synthesis of *in situ* reduced metal Bi decorated bismuth molybdate hollow microspheres with enhancing photocatalytic activity, *Appl. Surf. Sci.* 396 (2017) 438–443.

[58] M. Besson, P. Gallezot, Selective oxidation of alcohols and aldehydes on metal catalysts, *Catal. Today* 57 (2010) 127–141.

[59] Y. Kwon, Y. Birdja, I. Spanos, P. Rodriguez, M.T.M. Koper, Highly selective electro-oxidation of glycerol to dihydroxyacetone on platinum in the presence of bismuth, *ACS Catal.* 2 (2012) 759–764.